International Journal of Plasticity 26 (2010) 1792–1805

Contents lists available at ScienceDirect

International Journal of Plasticity

journal homepage: www.elsevier.com/locate/ijplas

Compliant interfaces: A mechanism for relaxation of dislocation pile-ups in a sheared single crystal

K. Danas *, V.S. Deshpande, N.A. Fleck

Centre for Micromechanics, Department of Engineering, University of Cambridge, Trumpington Street, Cambridge CB2 1PZ, UK

ARTICLE INFO

Article history:
Received 12 November 2009
Received in final revised form 24 March 2010
Available online 2 April 2010

Keywords:
Discrete dislocations
Size effects
Strain-gradient plasticity
Interfaces
Crystal plasticity

ABSTRACT

Discrete dislocation plasticity models and strain-gradient plasticity theories are used to investigate the role of interfaces in the elastic–plastic response of a sheared single crystal. The upper and lower faces of a single crystal are bonded to rigid adherends via interfaces of finite thickness. The sandwich system is subjected to simple shear, and the effect of thickness of crystal layer and of interfaces upon the overall response are explored. When the interface has a modulus less than that of the bulk material, both the predicted plastic size effect and the Bauschinger effect are considerably reduced. This is due to the relaxation of the dislocation stress field by the relatively compliant surface layer. On the other hand, when the interface has a modulus equal to that of the bulk material a strong size effect in hardening as well as a significant reverse plasticity are observed in small specimens. These effects are attributed to the energy stored in the elastic fields of the geometrically necessary dislocations (GNDs).

1. Introduction – experimental motivation

Recently, size effects have been observed in the plastic deformation of structures in the micron range (Fleck et al., 1994; Hutchinson, 2000). The underlying concept is that plastic strain gradients lead to the enhancement in the density of geometrically necessary dislocations and thereby to an elevation in material strength. Consequently, "smaller is stronger".

The presence of strain gradients can be an inevitable consequence of the test configuration, regardless of the imposed boundary conditions: strain gradients are present in a beam under bending, a wire in torsion, in the vicinity of an indentation in a solid and near a crack tip. In other circumstances, the existence of plastic strain gradients requires a particular set of imposed boundary conditions. For example, grain boundaries in a polycrystal can impede slip and thereby result in a Hall–Petch size effect (Aifantis and Willis, 2005; Borg and Fleck, 2007). Surface passivation of thin films in tension can also impede dislocation motion at the surface and thereby generate strain gradients (Xiang and Vlassak, 2006). Likewise, the plastic shearing of a single crystal sandwiched between elastic adherends can lead to the pile-up of dislocations on inclined slip planes and thereby induce a plastic strain gradient. A number of numerical studies suggest that the blockage of dislocations at the crystal–substrate interface leads to both isotropic and kinematic hardening: the macroscopic shear strength increases with diminishing layer thickness (Shu et al., 2001; Gurtin and Needleman, 2005). These studies treat the crystal–substrate interface as "perfectly hard".

In reality, the "hard interface" assumption may over-emphasise the role of strain gradient strengthening in a sandwich layer. This is supported by recent measurements performed by Tagarielli and Fleck (in preparation) on the shear strength of a thin aluminium layer sandwiched between sapphire blocks. These authors find a negligible effect of layer thickness upon

* Corresponding author. Present address: Laboratoire de Mécanique des Solides, C.N.R.S. UMR7649, Département de Mécanique, École Polytechnique, 91128 Palaiseau Cedex, France.
E-mail addresses: kd301@cam.ac.uk, kdanas@lms.polytechnique.fr, kosdanas@gmail.com (K. Danas), vsd@eng.cam.ac.uk (V.S. Deshpande), naf1@cam.ac.uk (N.A. Fleck).

0749-6419/$ - see front matter © 2010 Elsevier Ltd. All rights reserved.
doi:10.1016/j.ijplas.2010.03.008

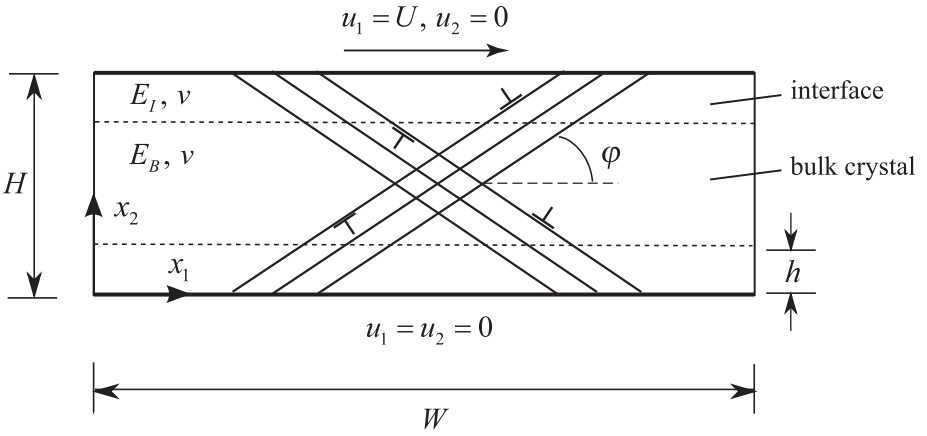

Fig. 1. Sketch of the boundary value problem.

the macroscopic shear strength for layers of thickness 10–50 μm. Given that strong strain gradients will exist in the specimen when dislocations are not permitted to exit from the adhered boundaries, one possible explanation for this negligible size effect is that interfaces can relax the stress fields of dislocations in the vicinity of the interface. Consequently, the hardening contribution (and associated Bauschinger effect) due to pile-ups are significantly reduced. The aim of the present study is to explore the sensitivity of size effects in thin sheared layers to the compliance of the interface. Both discrete dislocation and strain gradient crystal plasticity approaches are employed.

Consider the simple shear of a prototypical single crystal with two symmetric slip systems, with slip planes orientated at angles $\varphi^{(1)} = -\varphi^{(2)} = \varphi$ with respect to the x_1-axis as shown in Fig. 1. The crystal is sandwiched between two rigid blocks, and the blocks are subjected to a relative sliding displacement. Dislocation sources will be activated and dislocations will glide under the applied load on both slip systems until they impinge the rigid blocks. If the interfaces are perfectly bonded and of vanishing thickness, the dislocations will pile-up and generate long-range elastic back-stresses. This will impede further dislocation activity and will result in both strong macroscopic hardening and a Bauschinger effect.

It is likely, however, that manufacture of the sandwich specimen (e.g., the joining of two dissimilar solids by diffusion bonding) will generate an interface of finite thickness, and with an internal structure that is more amorphous than that of the bulk and consequently more compliant. In turn, this will result in the relaxation of stresses in the dislocation pile-ups. The principal aim of the current study is to use discrete dislocation simulations to explore the significance of interface compliance upon the elastic–plastic response of the sandwiched single crystal under remote shear. The ability of strain-gradient plasticity theory to mimic the discrete dislocation behaviour is also investigated. It is recognised that current discrete dislocation simulations do not account for a number of phenomena that occur deep in the plastic range, for example, forest hardening and cross-slip. These additional effects can be modelled in an approximate manner using strain-gradient plasticity theory: this is done in the final section of the paper.

1.1. Specification of the sandwiched single crystal

A specimen crystal of overall height H comprises a single crystal bonded to rigid blocks via interfaces, each of height h, as shown in Fig. 1. Following numerous other studies in crystal plasticity (e.g., see review by Asaro (1983) and manuscript by Nye (1957)), we attempt to model a crystal that is representative of FCC aluminium. Thus, we assume that the crystal is elastically isotropic but plastically anisotropic with two slip systems[1] with slip planes aligned at $\varphi^{(1)} = -\varphi^{(2)} = 30^\circ$. This scheme whereby the plastic anisotropy is modelled but the elastic anisotropy neglected has been demonstrated in numerous studies to qualitatively capture the shear response of a sandwiched single crystal (see for instance Shu et al. (2001)). Both interfaces share the same slip systems as those of the bulk crystal. Consequently, dislocations that have been generated within the bulk are able to glide into the interfaces. However, it is envisaged that the interfaces have a reduced elastic modulus compared to that of the bulk and so the stress field associated with each dislocation in the interface is diminished.

Use the subscript B to denote the bulk crystal, and the subscript I to denote the interface. Then, the Young's modulus of the bulk crystal and interface are E_B and E_I, respectively (the Poisson ratio ν is taken to be the same for both solids). The slip direction vector $s_i^{(\alpha)}$ and plane unit normal $m_i^{(\alpha)}$ of each slip system α is

$$s_i^{(\alpha)} = \cos\varphi^{(\alpha)} e_i^{(1)} + \sin\varphi^{(\alpha)} e_i^{(2)}, \quad m_i^{(\alpha)} = -\sin\varphi^{(\alpha)} e_i^{(1)} + \cos\varphi^{(\alpha)} e_i^{(2)}, \tag{1}$$

where $e_i^{(1)}$ and $e_i^{(2)}$ are unit vectors along the x_1 and x_2 axes, respectively.

[1] This choice of slip systems models plane-strain deformation involving simultaneous and equal shear on the pair of planes $(\bar{1}\,1\,1)$ and $(1\,1\,\bar{1})$ as discussed by Rice (1987).

The crystal is subjected to plane-strain conditions in the x_3-direction, i.e., $\varepsilon_{i3} = 0$ ($i = 1,2,3$). Simple shear loading is applied on the upper and lower surfaces with $u_1 = U$ at $x_2 = H$ and $u_1 = 0$ at $x_2 = 0$ such that the imposed macroscopic shear strain is $\Gamma = U/H$. Full constraint is imposed in the x_2 direction such that $u_2 = 0$ along $x_2 = 0$ and $x_2 = H$. On the lateral faces, we apply periodic boundary conditions, i.e., $\Delta u_i = 0$, where Δu_i is the difference between displacements on opposite sides of the crystal.

2. Constitutive modelling

Two complementary formulations are used to predict the response of the sandwich layer shown in Fig. 1:

(I) the discrete dislocation plasticity formulation of Van der Giessen and Needleman (1995), and
(II) a generalisation of the strain-gradient crystal plasticity theory of Gurtin (2002) along the lines proposed by Fleck and Willis (2009b). The corresponding constitutive laws for the bulk and the interfaces are chosen to match the discrete dislocation simulations for specimens of large height H.

2.1. Discrete dislocation plasticity

Following the pioneering work of Van der Giessen and Needleman (1995) and subsequent studies by Deshpande and coworkers (Deshpande et al., 2002; Deshpande et al., 2002; Balint et al., 2005; Hussein et al., 2008), we describe briefly a numerical framework, labelled as DD, where full boundary value problem solutions are obtained by consideration of the collective motion of a large number of edge dislocations (or line singularities) in an elastic medium inducing plastic flow.

In the present study, the dislocation structure within the bulk crystal involves the nucleation and motion of dislocations, their mutual annihilation and their pinning at random obstacles. Although the interfaces are free of sources and obstacles, dislocations are able to glide into them from the bulk. In addition, the interfaces are allowed to have a different Young's modulus than that of the bulk, as suggested in the Introduction.

The loading is applied incrementally. At each increment, the stress and deformation state are computed by superposition of the singular dislocation field and the image field. The singular field ($\tilde{}$) associated with N dislocations is calculated analytically from the isotropic linear elastic dislocation fields in an infinite medium (Hirth and Lothe, 1968). The complete solution is obtained by adding a smooth image field ($\hat{}$) that ensures that the boundary conditions are satisfied. The displacements u_i, strains ε_{ij}, and stresses σ_{ij} are given by

$$u_i = \widehat{u}_i + \widetilde{u}_i, \quad \varepsilon_{ij} = \widehat{\varepsilon}_{ij} + \widetilde{\varepsilon}_{ij}, \quad \sigma_{ij} = \widehat{\sigma}_{ij} + \widetilde{\sigma}_{ij}, \tag{2}$$

where the ($\tilde{}$) field is the sum of the fields due to the presence of N individual dislocations in their current positions, i.e.,

$$\widetilde{u}_i = \sum_{J=1}^{N} \widetilde{u}_i^{(J)}, \quad \widetilde{\varepsilon}_{ij} = \sum_{J=1}^{N} \widetilde{\varepsilon}_{ij}^{(J)}, \quad \widetilde{\sigma}_{ij} = \sum_{J=1}^{N} \widetilde{\sigma}_{ij}^{(J)}. \tag{3}$$

The image field ($\hat{}$) is obtained by solving a linear elastic boundary value problem using finite elements with the boundary conditions changing as the dislocation structure evolves. When the solution domain comprises phases with different elastic moduli, as in the case here, a polarisation term is included in the finite element calculation of the ($\hat{}$) fields as elaborated in Van der Giessen and Needleman (1995).

Further, recall that the boundary value problem being solved is periodic in the x_1 direction with period W. The ($\tilde{}$) fields for the dislocations are the analytical fields in an infinite medium and hence not periodic. Periodicity of the total fields is enforced via the ($\hat{}$) fields, i.e., while both ($\hat{}$) and ($\tilde{}$) fields are not periodic, their sum is periodic in the x_1 direction with period W. In addition to the periodicity of the u fields, the tractions are also set to be anti-periodic (Michel et al., 1999). Note however that since the ($\tilde{}$) tractions derived by the dislocation fields are not anti-periodic, the ($\hat{}$) tractions will not be anti-periodic either.

At the beginning of the calculation, the crystal is stress- and dislocation-free. Long range interactions of the dislocations arise automatically from their elastic fields while the following constitutive rules account for short range interactions:

(i) Dislocation dipoles with Burgers vectors $\pm \mathbf{b}$ are nucleated at point sources, that simulate Frank–Read sources, randomly distributed on the discrete slip planes. Nucleation occurs when the magnitude of the resolved shear stress at the source exceeds a critical value τ_{nuc} during a time period t_{nuc}. The sign of the dipole is determined by the sign of the resolved shear stress along the slip plane while the distance between the two dislocations at nucleation, L_{nuc}, is taken such that the attractive stress that the dislocations exert on each other is equilibrated by a shear stress of magnitude τ_{nuc}.
(ii) After nucleation, the dislocations glide apart, driven by the Peach–Koehler force acting on them, given by

$$f^{(I)} = m_i^{(I)} \left[\widehat{\sigma}_{ij} + \sum_{J \neq I} \widetilde{\sigma}_{ij}^{(J)} \right] b_j^{(I)}, \tag{4}$$

where $m_i^{(I)}$ is the unit normal to the slip system on which the dislocation with Burgers vector $b_j^{(I)}$ resides. The magnitude of the glide velocity $V_g^{(I)}$ along the slip direction of the dislocation I is taken to be linearly related to the Peach–Koehler force $f^{(I)}$ through the drag relation $V_g^{(I)} = f^{(I)}/B$ with B denoting the drag coefficient.

(iii) Annihilation of two opposite signed dislocations on a slip plane occurs when they are within a material-dependent critical annihilation distance L_e.
(iv) The obstacles to dislocation motion are modelled as randomly distributed points on the slip planes such that when dislocations attempt to pass through them they are pinned. An obstacle releases a pinned dislocation when the Peach–Koehler force on the obstacle exceeds $\tau_{obs}b$, where τ_{obs} is the obstacle strength and b is the magnitude of the Burgers vector.

These constitutive rules are typically only valid during stage I of the crystal response wherein forest hardening effects are negligible. Augmented rules suggested by Benzerga et al. (2004) can incorporate forest hardening effects in a two-dimensional, DD simulation but are not required here since we restrict our analysis to stage I deformations.

2.2. Strain-gradient crystal plasticity

In this section, we describe a strain-gradient crystal plasticity formulation, labelled as SGP, which is based on the principle of virtual work introduced by Gurtin (2002) (see also Borg (2007), Borg and Fleck (2007)). The constitutive relations are motivated by the recent strain-gradient plasticity model of Fleck and Willis (2009b).

2.2.1. Kinematics

The total strain-rate tensor is defined as the symmetric part of the rate of displacement and is written as

$$\dot{\varepsilon}_{ij} = \frac{1}{2}(\dot{u}_{i,j} + \dot{u}_{j,i}) = \dot{\varepsilon}^e_{ij} + \dot{\varepsilon}^p_{ij}, \tag{5}$$

with $\dot{\varepsilon}^e_{ij}$ and $\dot{\varepsilon}^p_{ij}$ denoting the elastic and plastic strain-rate, respectively. Plastic deformation is due to slip on slip systems defined by the slip plane normal, $m^{(\alpha)}_i$, and the slip direction $s^{(\alpha)}_i$, as defined in relation (1). Making use of the slip rate $\dot{\gamma}^{(\alpha)}_p$ on a specific slip system α, we define the plastic strain-rate as

$$\dot{\varepsilon}^p_{ij} = \sum_{\alpha} \dot{\gamma}^{(\alpha)}_p \mu^{(\alpha)}_{ij}, \tag{6}$$

where $\mu^{(\alpha)}_{ij} = (s^{(\alpha)}_i m^{(\alpha)}_j + m^{(\alpha)}_i s^{(\alpha)}_j)/2$ is the Schmid orientation tensor.

2.2.2. Principle of virtual work

Let S and V denote the exterior surface and the volume of the specimen under study. Write $q^{(\alpha)}$ as a stress measure work-conjugate to the slip rate $\dot{\gamma}^{(\alpha)}_p$, $\tau^{(\alpha)}_i$ as a higher order stress measure work-conjugate to the gradient of the slip rate $\dot{\gamma}^{(\alpha)}_{p,i}$ (where the subscript $(\,)_{,i}$ denotes partial derivatives with respect to the spatial coordinate x_i), σ_{ij} as the Cauchy stress work conjugate to the elastic strain ε^e_{ij} and write $\sigma^{(\alpha)} = \sigma_{ij}\mu^{(\alpha)}_{ij}$ as the Schmid stress. T_i and $t^{(\alpha)}$ are the traction and higher order traction, work-conjugate to the displacement rate $\dot{u}_i$ and the slip rate $\dot{\gamma}^{(\alpha)}_p$, respectively. Then, the principle of virtual work states (Gurtin, 2002; Borg, 2007; Borg and Fleck, 2007)

$$\int_V \left[\sigma_{ij}\delta\dot{\varepsilon}_{ij} + \sum_{\alpha}\left(q^{(\alpha)} - \sigma^{(\alpha)}\right)\delta\dot{\gamma}^{(\alpha)}_p + \sum_{\alpha}\tau^{(\alpha)}_i\delta\dot{\gamma}^{(\alpha)}_{p,i}\right]\mathrm{d}V = \int_S \left(T_i\delta\dot{u}_i + \sum_{\alpha} t^{(\alpha)}\delta\dot{\gamma}^{(\alpha)}_p\right)\mathrm{d}S, \tag{7}$$

where $\delta(\cdot)$ denotes an arbitrary variation in $(\cdot)$.

Integration by parts of (7) leads to the strong form of the field equations:

$$\sigma_{ij,j} = 0, \quad q^{(\alpha)} - \tau^{(\alpha)}_{i,i} = \sigma^{(\alpha)}, \quad \text{in} \quad V \tag{8}$$

for each slip plane α. These macroscopic and microscopic force balances are complemented with the equilibrium statements on the boundary,

$$T_i = \sigma_{ij}n_j, \quad t^{(\alpha)} = \tau^{(\alpha)}_i n_i, \quad \text{on} \quad S, \tag{9}$$

where n_i is the outward unit normal to the surface S.

2.2.3. Constitutive equations

A viscoplastic formulation is now presented for the dependence of $(q^{(\alpha)}, \tau^{(\alpha)}_i)$ upon $\dot{\gamma}^{(\alpha)}_p$, $\gamma^{(\alpha)}_p$ and their spatial gradients. In the strain gradient formulation, the values adopted for the material parameters in the bulk crystal are chosen in order to reproduce the discrete dislocation results. There remains some choice of values for the interfaces. Precisely the same constitutive laws and numerical values are assumed for the interface and bulk crystal, with the following exceptions: (i) the Young's modulus of the interface is allowed to deviate from the bulk value as done in the discrete dislocation simulations, and (ii) the energetic length scale for the interface (to be made precise below) is calibrated to a different value from that of the bulk in order to closely mimic the discrete dislocation results.

Following the recent work of Fleck and Willis (2009a, b), we propose phenomenological constitutive laws for the "energetic" and "dissipative" parts of $(q^{(\alpha)}, \tau^{(\alpha)}_i)$. More specifically, the stored internal energy of the medium U consists of the conventional elastic energy U_e and a defect energy U_p which is attributed to the energy stored in the elastic fields of the

geometrically necessary dislocations (GNDs) (Ashby, 1970; Fleck et al., 1994; Gurtin, 2002) and is expected to be important at small length scales. Assuming that U_e and U_p are uncoupled, one may write, in general, that

$$U(\varepsilon^e_{ij}, \gamma^{(\alpha)}_p, \gamma^{(\alpha)}_{p,i}) = U_e(\varepsilon^e_{ij}) + U_p(\gamma^{(\alpha)}_p, \gamma^{(\alpha)}_{p,i}). \tag{10}$$

The elastic energy U_e and the Cauchy stress $\sigma_{ij} = \partial U_e/\partial \varepsilon^e_{ij}$ are expressed for an isotropic solid as

$$U_e(\varepsilon^e_{ij}) = \frac{E}{2(1+\nu)}\left(\varepsilon^e_{ij}\varepsilon^e_{ij} + \frac{\nu}{1-2\nu}(\varepsilon^e_{kk})^2\right), \quad \sigma_{ij} = \frac{E}{1+\nu}\left(\varepsilon^e_{ij} + \frac{\nu}{1-2\nu}\varepsilon^e_{kk}\delta_{ij}\right), \tag{11}$$

where δ_{ij} is the second-order identity tensor (Krönecker delta). For simplicity, we assume no cross-coupling from one slip system to the next and write the defect energy U_p as

$$U_p(\gamma^{(\alpha)}_p, \gamma^{(\alpha)}_{p,i}) = \sum_\alpha U^{(\alpha)}_p(\gamma^{(\alpha)}_p, \gamma^{(\alpha)}_{p,i}), \tag{12}$$

where $U^{(\alpha)}_p$ are the defect energies of each slip system. It remains to specify a particular functional form for $U^{(\alpha)}_p$. It is convenient to first introduce an effective slip measure (homogeneous of degree one in its arguments)

$$\gamma^{(\alpha)}_e = \left[\Theta|\gamma^{(\alpha)}_p|^\rho + |L\gamma^{(\alpha)}_{p,i}s^{(\alpha)}_i|^\rho\right]^{1/\rho}, \tag{13}$$

with $0 < \rho < \infty$ and L denoting an energetic length scale parameter which in general is different for the bulk crystal and interface, whereas $\Theta = \{1,0\}$ is a flag that is used to either turn on or off, respectively, the dependence on $\gamma^{(\alpha)}_p$ (see Section 3.4 for the physical significance of Θ). Making use of (13), we propose a defect energy $U^{(\alpha)}_p$ of the form

$$U^{(\alpha)}_p(\gamma^{(\alpha)}_e) = \frac{\beta G}{M+1}\left(\gamma^{(\alpha)}_e\right)^{M+1} \quad \text{or} \quad U'^{(\alpha)}_p(\gamma^{(\alpha)}_e) = \beta G\left(\gamma^{(\alpha)}_e\right)^M, \tag{14}$$

where the prime denotes the derivative with respect to the argument of the function, β is a scalar constant and $G = E/(2+2\nu)$ denotes the shear modulus. When $M = 1$ (a value to be adopted in the following calculations), (14) is quadratic in $\gamma^{(\alpha)}_e$ and thus has a similar form to the one proposed by Gurtin (2002).

Similarly, we introduce an effective slip rate for plastic dissipation (homogeneous of degree one in its arguments) such that

$$\dot\gamma^{(\alpha)}_e = \left[|\dot\gamma^{(\alpha)}_p|^\mu + |l\dot\gamma^{(\alpha)}_{p,i}s^{(\alpha)}_i|^\mu\right]^{1/\mu}, \tag{15}$$

where $0 < \mu < \infty$ and l denotes a dissipative length scale. Assuming that both the bulk and interface materials exhibit rate-dependent (viscoplastic) behaviour, with no dissipative hardening, a power-law dissipation potential ϕ is introduced as

$$\phi^{(\alpha)}(\dot\gamma^{(\alpha)}_e) = \frac{\sigma_y\dot\gamma_o}{m+1}\left(\frac{\dot\gamma^{(\alpha)}_e}{\dot\gamma_o}\right)^{m+1} \quad \text{or} \quad \phi'^{(\alpha)}(\dot\gamma^{(\alpha)}_e) = \sigma_y\left(\frac{\dot\gamma^{(\alpha)}_e}{\dot\gamma_o}\right)^m. \tag{16}$$

Here, σ_y is a flow strength, $\dot\gamma_o$ is a reference slip rate, m is the strain-rate sensitivity parameter taking values between 1 (linear viscoelasticity) and 0 (rate-independent limit or perfect plasticity).

Next, we present the constitutive relations between the stress and strain variables. The quantities $q^{(\alpha)}$ and $\tau^{(\alpha)}_i$ are partitioned into dissipative, $(.)^D$, and energetic, $(.)^E$, parts (Fleck and Willis, 2009b) such that

$$\tau^{(\alpha)}_i = \tau^{E(\alpha)}_i + \tau^{D(\alpha)}_i, \quad q^{(\alpha)} = q^{E(\alpha)} + q^{D(\alpha)}. \tag{17}$$

Then, upon making use of relations (13)–(16), the energetic stresses read

$$\begin{aligned} q^{E(\alpha)} &= \frac{\partial U^{(\alpha)}_p}{\partial \gamma^{(\alpha)}_p} = \Theta U'^{(\alpha)}_p \frac{|\gamma^{(\alpha)}_p|^{\rho-2}}{\left(\gamma^{(\alpha)}_e\right)^{\rho-1}}\gamma^{(\alpha)}_p, \\ \tau^{E(\alpha)}_i &= \frac{\partial U^{(\alpha)}_p}{\partial \gamma^{(\alpha)}_{p,i}} = L^2 U'^{(\alpha)}_p \frac{|L\gamma^{(\alpha)}_{p,k}s^{(\alpha)}_k|^{\rho-2}}{(\gamma^{(\alpha)}_e)^{\rho-1}}\left(\gamma^{(\alpha)}_{pj}s^{(\alpha)}_j\right)s^{(\alpha)}_i, \end{aligned} \tag{18}$$

while the dissipative stresses are

$$\begin{aligned} q^{D(\alpha)} &= \frac{\partial \phi^{(\alpha)}}{\partial \dot\gamma^{(\alpha)}_p} = \phi'^{(\alpha)} \frac{|\dot\gamma^{(\alpha)}_p|^{\mu-2}}{\left(\dot\gamma^{(\alpha)}_e\right)^{\mu-1}}\dot\gamma^{(\alpha)}_p, \\ \tau^{D(\alpha)}_i &= \frac{\partial \phi^{(\alpha)}}{\partial \dot\gamma^{(\alpha)}_{p,i}} = l^2\phi'^{(\alpha)} \frac{|l\dot\gamma^{(\alpha)}_{p,k}s^{(\alpha)}_k|^{\mu-2}}{\left(\dot\gamma^{(\alpha)}_e\right)^{\mu-1}}\left(\dot\gamma^{(\alpha)}_{pj}s^{(\alpha)}_j\right)s^{(\alpha)}_i, \end{aligned} \tag{19}$$

The strain gradient formulation for the sandwiched sheared crystal leads to a non-linear set of ODEs in rate quantities as a function of x_2. A solution is obtained by the finite element method using an one-dimensional setup similar to those of Gurtin (2002) and Borg (2007) (not repeated here).

3. Results and discussion

First, results are given for the DD simulations. Material properties are chosen to be representative of aluminium single crystals (Kubin et al., 1992) albeit with some modifications to parameters like source density and slip plane spacing, in order to allow computations to be carried out in the 1–5 μm range rather than the 10–50 μm range which makes the DD calculations computationally prohibitive. A sensitivity analysis is performed of the macroscopic response to the following prime variables: H, h and E_I/E_B. In this way, the dependence of the size effect in shear response and the properties of the interface is determined. Second, the ability of the strain gradient calculations to mimic the DD results is assessed. Third, the degree of Bauschinger effect is investigated for both the DD and SGP formulations. And finally, a broad scoping exercise is performed in order to reveal the relationship between the macroscopic shear response and each of the constitutive ingredients in the SGP formulation; for example, the relative significance of dissipative and energetic terms is explored.

3.1. The DD simulations for forward loading

The Young's modulus of the bulk material is taken as $E_B = 70$ GPa, whereas the Young's modulus E_I of the interface material is ascribed the selected values of $E_I/E_B = 1, 0.5, 0.25, 0.1$. The Poisson ratio $\nu = 0.3$ is identical for both solids, and the shear moduli of the bulk and the interfaces are given by the standard isotropic relations $G_B = E_B/(2+2\nu)$ and $G_I = E_I/(2+2\nu)$, respectively.

We consider crystals of total height $H = 0.5, 0.7, 1, 2, 4$ μm and width $W = 3H$ and three different interface heights $h = 0.1$, 0.05, 0 μm. Following numerous earlier studies (e.g., Van der Giessen and Needleman (1995), Shu et al. (2001), Hussein et al. (2008)) we have chosen the following parameter set for the DD calculations. All slip planes have a spacing $100b$ with the magnitude of the Burger's vector held fixed at $b = 0.25$ nm for all dislocations. The Frank–Read sources and obstacles are randomly distributed with a density $\rho_{nuc} = \rho_{obs} = 20\ \mu m^{-2}$. Each source is randomly assigned a nucleation strength from a Gaussian distribution with average $\bar{\tau}_{nuc} = 50$MPa and standard deviation $\Delta\tau_{nuc} = 10$ MPa while the nucleation time is $t_{nuc} = 10$ ns for all sources. The obstacle strength is $\tau_{obs} = 150$ MPa. The drag coefficient associated with the dislocation motion is $B = 10^{-4}$Pa · s and the annihilation distance is $L_e = 6b$. Finally, the DD results are obtained by averaging over five realisations of source and obstacle distributions. We emphasise that the bulk material contains sources and obstacles whereas the interfaces are free of both sources and obstacles and all calculations are conducted for an applied shear strain-rate $\dot{\Gamma} = 2000\ s^{-1}$ and a time step $\Delta t = 0.5$ ns.

Fig. 2 shows DD shear stress–strain curves for H in the range of 0.5–4 μm and $h = 0.1$ μm. Here (and subsequently), the shear stress is the remote applied stress that is conjugate to the imposed macroscopic shear strain Γ. The moduli ratio equals $E_I/E_B = 1$ in part (a) and $E_I/E_B = 0.25$ in part (b). It is clear from Fig. 2a that the smaller crystals ($H < 1$ μm) exhibit a significant size effect in hardening, which gradually decreases for larger crystals. The observed hardening has an energetic character (as will be seen below where unloading is considered) and is attributed to the fact that the fixed upper and lower surfaces (passivated boundary) do not allow the dislocations to exit the crystal, thus creating dislocation pile-ups near the boundaries of the crystal. These dislocation pile-ups generate long-range elastic back-stresses which impede further dislocation activity in the crystal. This in turn leads to the development of strong plastic-strain gradients near the upper and lower boundaries and

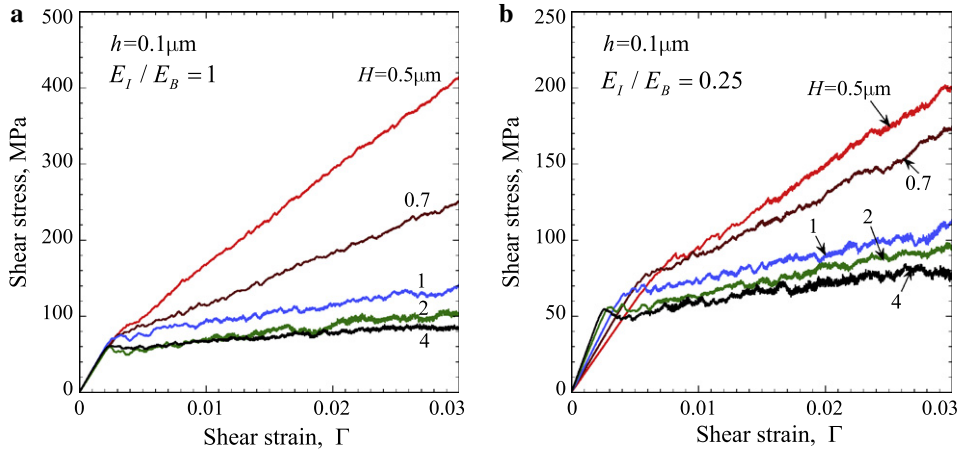

Fig. 2. DD shear stress–strain curves for $H = 0.5, 0.7, 1, 2, 4$ μm and $h = 0.1$ μm for (a) $E_I/E_B = 1$ and (b) $E_I/E_B = 0.25$.

to an increase of the overall shear strength. In contrast, no significant size effect is observed for the initial yield point. Upon reducing the Young's modulus of the interface, the macroscopic shear strength reduces significantly; compare parts (a) and (b) of the figure paying attention to the different scales. The reduced Young's modulus of the interface induces much lower back-stresses in the bulk solid, leading to a relaxation of the macroscopic shear stress in the single crystal.

The effect of interface modulus upon the macroscopic shear response is shown explicitly in Fig. 3 for (a) $H = 0.5\mu$m and (b) $H = 2$ μm, with h held fixed at $h = 0.1$ μm. For the choice (a) of $H = 0.5$ μm the interface comprises a significant fraction of the layer height, and the strain hardening response is sensitive to the value of E_I/E_B. On the other hand, the interface comprises a minor proportion of the layer height for the choice $H = 2$ μm in part (b) and its presence has a negligible effect upon the macroscopic shear response for all E_I/E_B. For large H, the behaviour of the crystal is dominated by the motion of dislocations in the bulk.

3.2. Calibration of the strain-gradient plasticity model against the DD results for forward loading

The SGP theory contains a number of parameters that require calibration against the DD results reported above. Some are obvious: the Young's modulus and Poisson ratio are the same as those used in the DD simulations. It remains to specify the flow strength, material length scales, strain-rate sensitivity and internal defect energy. Here, we do not attempt to make a formal link between the DD and continuum theory parameters. Rather, the parameters of the SGP theory (e.g., flow strength, strain hardening, etc.) are chosen so as to reproduce the DD simulations in a consistent manner while not trying to make the connection between these continuum parameters and the underlying physical phenomena such as cross-slip and forest hardening. We specify $M = 1$ and $\beta = 0.25$ in order to obtain a linear strain hardening characteristic in the SGP calculations. We now argue that we need to set $\Theta = 0$ in (13) in order to switch off the macroscopic strain hardening at large H, as observed in Figs. 2 and 3 (see Section 3.4 for a detailed discussion on the various terms of the SGP model). Then, expression $(18)_2$ reduces to

$$\tau_i^{E(\alpha)} = \frac{G}{4} L^2 \gamma_{p,j}^{(\alpha)} s_j^{(\alpha)} s_i^{(\alpha)}, \tag{20}$$

while $q^{E(\alpha)} = 0$. This allows for macroscopic strain hardening at small H but not for large H.

In order to define the flow strength σ_y as well as the strain-rate sensitivity parameter m, introduced in the constitutive relation (16), we make use of the DD shear response for a crystal with $H = 4$ μm, $h = 0.1$ μm and $E_I/E_B = 1$ as shown in Fig. 2a. The SGP formulation is brought into line with the DD prediction by taking a flow strength $\sigma_y = 30$ MPa, a strain-rate sensitivity $m = 0.05$, a reference slip rate $\dot{\gamma}_o = 10^{-3}\ s^{-1}$ combined with an applied shear strain-rate $\dot{\Gamma} = 10^{-3}\ s^{-1}$.

The power μ in (15) is chosen as $\mu = 2$ (Fleck and Hutchinson, 2001). Note that the SGP theories require also the prescription of boundary conditions for the plastic slip rate. In the present study, we set $\dot{\gamma}_p^{(\alpha)} = 0$ at $x_2 = 0$ and $x_2 = H$ (Gurtin, 2002). Such a boundary condition mimics the fact that dislocations are blocked by the rigid adherends.

Next, we ascribe values to the dissipative length scales, l_B and l_I, and to the energetic length scales L_B and L_I. Following Shu et al. (2001) and Hussein et al. (2008), we choose $l_B = l_I = L_B = 10^3 b = 0.25$ μm. It remains to select a value for the energetic length scale of the interface L_I. Recall that no sources are introduced in the interfaces in the DD calculations. This suggests that L_I is larger than L_B. We shall subsequently show that the choice $L_I = 2L_B$ gives good agreement between the SGP and DD predictions.

Fig. 4 presents DD and SGP shear stress–strain loading curves for (a) a crystal of small height $H = 0.5$ μm and (b) a crystal of large height $H = 2$ μm with interface heights $h = 0.1, 0.05, 0$ μm and a Young's moduli ratio $E_I/E_B = 1$. For case (a), the degree

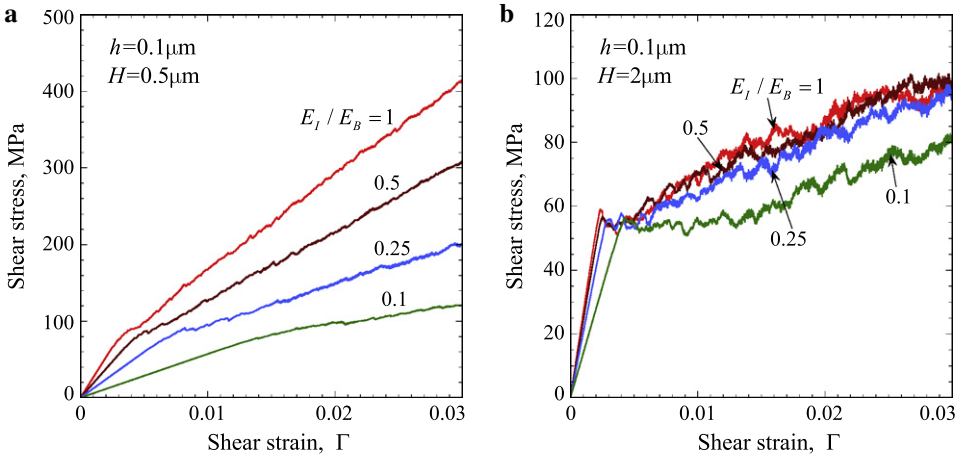

Fig. 3. DD shear stress–strain curves for $E_I/E_B = 1, 0.5, 0.25, 0.1$ and $h = 0.1$ μm for (a) $H = 0.5$ μm and (b) $H = 2$ μm.

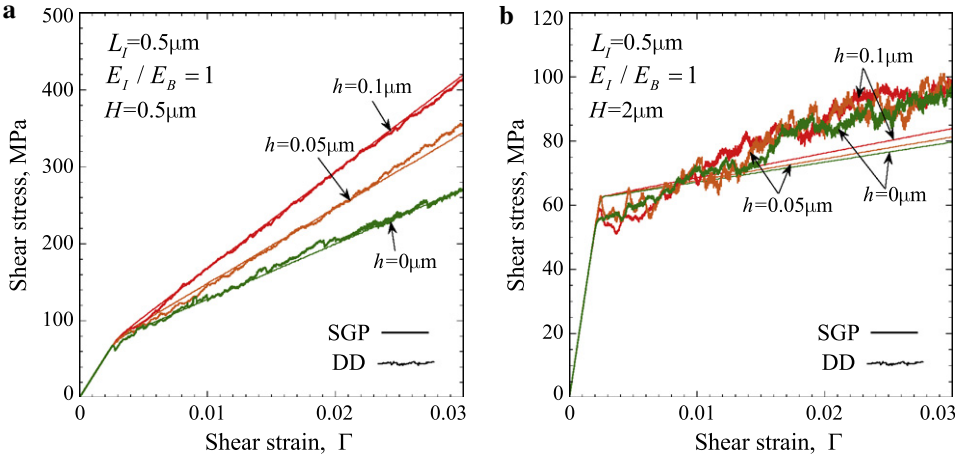

Fig. 4. DD vs. SGP stress–strain loading curves for (a) $H = 0.5\mu$m and (b) $H = 2$ μm for interface heights $h = 0.1$, 0.05, 0 μm and Young's moduli ratio $E_I/E_B = 1$.

of macroscopic strain hardening is sensitive to the value of h, due to the fact that the interface contains no sources and obstacles. The shear response is well-mimicked by the SGP theory upon making the choice $L_I = 2L_B$. (Had we set L_I equal to L_B, the SGP results would then show no dependence upon interface height and all curves would coincide with the $h = 0$ μm curve.) For case (b), the bulk response of the crystal dominates the behaviour and there is only a minor effect of the value of h upon the macroscopic DD behaviour. The SGP theory with $L_I = 2L_B$ captures this adequately with the nature of the discrepancies in part (b) not yet fully understood.

Many of the above results are conveniently summarised in Fig. 5 which presents plots for the macroscopic shear flow strength of the sandwich layer as predicted by the DD simulations (full circles) and the SGP formulation (continuous lines) for $H = 0.5$, 0.7, 1, 2, 4 μm and $h = 0.1$ μm as a function of the Young's moduli ratio E_I/E_B. In this figure, the flow strength is defined as the average macroscopic shear stress over the interval $0.01 \leqslant \Gamma \leqslant 0.02$. Excellent agreement is noted between the SGP and the DD simulations. It is clear from the figure that the degree of size effect progressively diminishes as the stiffness of the interface is reduced to a value much less than that of the bulk. For example, at $E_I/E_B = 1$ the flow strength increases by a factor of ~4 as H decreases from 4 to 0.5 μm. A significantly lower size effect occurs for a more compliant interface, i.e., $E_I/E_B = 0.1$. We further note that the flow strength is independent of the ratio E_I/E_B for large crystals.

Fig. 6 presents SGP results for the normalised plastic strain distribution γ_p/Γ at $\Gamma = 3\%$ along the thickness x_2/H of the specimen, where $\gamma_p \equiv 2\varepsilon^p_{12}$. Results are included for (a) $H = 0.5$ μm and (b) $H = 2$ μm and choices $E_I/E_B = 1$, 0.5, 0.25, 0.1. It is clear from Fig. 6a that the plastic strain distributions become increasingly more spatially uniform with decreasing E_I/E_B with the consequence that plastic strain gradients and hence size effects reduce with decreasing E_I/E_B. By contrast, the plastic strain distributions are less sensitive to E_I/E_B in the thicker specimen (Fig. 6b) and hence E_I/E_B plays a smaller role in the response of such specimens. We note that the average value of γ_p/Γ is approximately 0.3 across the thickness of the $H = 0.5$ μm specimen which means that elastic strains are comparable to the plastic strains even at the overall applied shear strain value

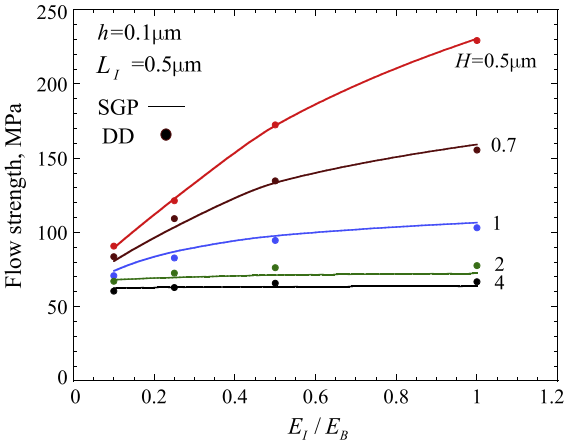

Fig. 5. Collective plots of the flow strength as predicted by the DD (full circles) and the SGP (continuous lines) for $H = 0.5$, 0.7, 1, 2 ,4 μm and $h = 0.1$ μm as a function of the Young's moduli ratio E_I/E_B. The flow strength is defined as the average macroscopic shear stress over the interval $0.01 \leqslant \Gamma \leqslant 0.02$.

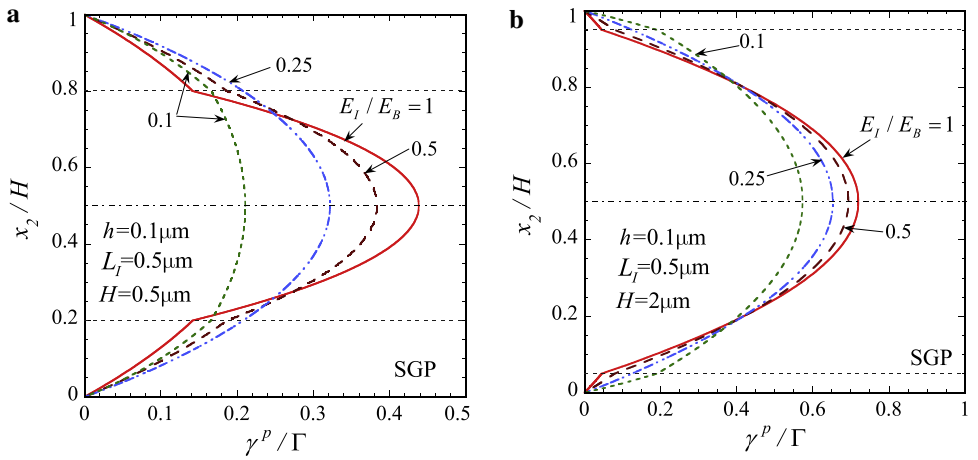

Fig. 6. SGP results of the normalised plastic strain γ_p/Γ at Γ = 3% along the height x_2/H for (a) H = 0.5 μm and (b) H = 2 μm. The interface regions are denoted with the dashed horizontal lines and results are included for E_l/E_B = 1, 0.5, 0.25, 0.1.

of Γ = 3%. This is due to the fact that high elastic back-stresses from dislocation pile-ups in the DD calculations significantly inhibit plasticity in this specimen.

3.3. The degree of Bauschinger effect according to the DD and SGP simulations

A series of simulations have been performed such that the loading direction undergoes a single reversal and the crystal is unloaded back to zero shear traction. Fig. 7 shows DD and SGP loading and unloading stress–strain curves with H = 0.5, 2 μm and h = 0.1 μm for (a) E_l/E_B = 1 and (b) E_l/E_B = 0.25. The SGP model captures remarkably well the hardening size effect and the unloading behaviour for both ratios E_l/E_B = 1, 0.25. For both values of E_l/E_B, the high strain hardening rate at H = 0.5 μm is mainly energetic in nature, and gives rise to a strong Bauschinger effect leading to a significant amount of reverse plasticity. This is in accord with the recent experimental observations of Xiang and Vlassak (2006) made in the context of thin films in tension with passivated surfaces.

In contrast, when H = 2 μm plasticity is mainly dissipative with negligible kinematic strain hardening, leading to (almost) linear elastic unloading. While the dissipative character is due to the motion of dislocations, the energetic behaviour of the crystal is attributed to the energy stored in the elastic fields of the GNDs. In the SGP calculations the energetic part of $\tau_i^{(\alpha)}$ (c.f. (17)) gives rise to the strong hardening of the stress–strain curve as well as to the large amount of reverse plasticity for the smaller specimen. On the other hand, as the crystal becomes larger, the dissipative components $q^{D(\alpha)}$ and $\tau_i^{D(\alpha)}$ dominate. At this point, we remind the reader that the energetic term $q^{E(\alpha)}$ has been set equal to zero since it would induce kinematic hardening even in the case of a large crystal, for example, $H \geqslant 4$ μm. The present DD simulations exhibit negligible hardening in this limiting case.

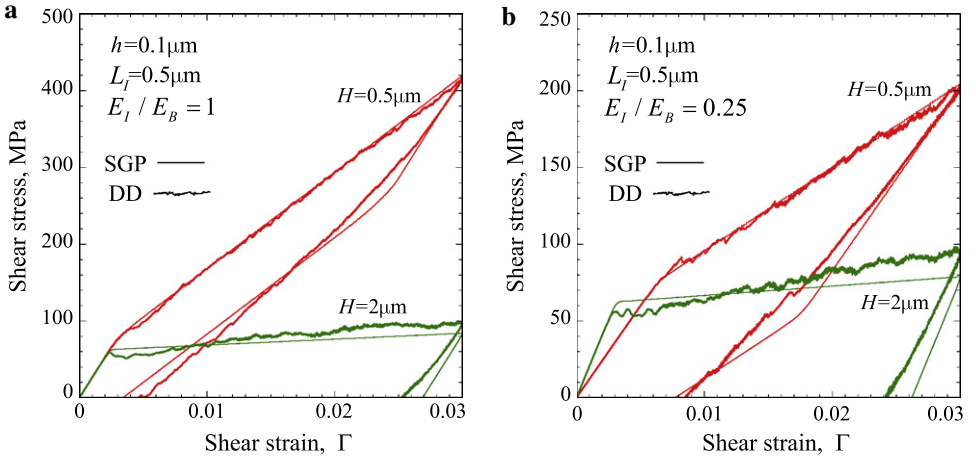

Fig. 7. DD vs. SGP loading and unloading stress–strain curves with H = 0.5, 2 μm, h = 0.1 μm for (a) E_l/E_B = 1 and (b) E_l/E_B = 0.25.

In order to further interrogate the Bauschinger effect, we introduce a normalised measure Γ_β of the amount of reverse plasticity present in the crystal after unloading. It is defined as follows. Load the crystal to a given shear traction and then fully unload the layer, as sketched in Fig. 8a. Denote the residual shear strain Γ upon full unloading by γ_{rp}, and write γ_{ep} as the average plastic shear strain that would be present if unloading was purely elastic. Then, the normalised measure of reversed plasticity is $\Gamma_\beta = \gamma_{rp}/\gamma_{ep}$. $\Gamma_\beta = 0$ denotes purely elastic unloading, implying a fully dissipative response of the crystal. In contrast, the extreme value of $\Gamma_\beta = 1$ denotes the case where the response to loading and unloading are dominated by purely energetic stresses, and zero plastic deformation remains upon full unloading.

The dependence of Γ_β at a maximum overall shear strain $\Gamma = 3\%$ upon the moduli ratio E_I/E_B is shown in Fig. 8b for $H = 0.5$, 0.7, 1, 2, 4 μm. Again, the SGP predictions are in excellent agreement with the DD values. For the small crystals, Γ_β increases rapidly as the ratio E_I/E_B is increased to the value of $\sim$0.6, and subsequently it approaches an asymptote for larger values of E_I/E_B. On the other hand, Γ_β is insensitive to the ratio E_I/E_B for the larger crystals taking very low values close to zero. These results again imply that dissipation is the main mechanism observed in large crystals whereas stored defect energy dominates the behaviour of smaller ones.

In view of the previously discussed unloading results, it is instructive to make a quantitative comparison between the average stored defect energy $\overline{U}_p$ of the DD and SGP simulations. While in the SGP formulation $\overline{U}_p$ is readily calculated by volume integration of relation (12) and (14), the evaluation of $\overline{U}_p$ in the DD simulations requires special attention. We first compute the total stored energy

$$\overline{U} = \frac{1}{V}\int_V \frac{1}{2}\sigma_{ij}\varepsilon_{ij}\mathrm{d}V, \tag{21}$$

over the volume V at each instant in time. Note that the dissipation in the DD simulations is a direct consequence of the motion of dislocations and therefore occurs between two subsequent time steps, i.e., when the dislocations move from one position to another with the help of the kinetic law (4). Consequently, the fields σ_{ij} and ε_{ij} defined in (2) contribute only to the total energy stored in the crystal. In turn, the elastic energy $\overline{U}_e$ due to the remote applied load is defined by

$$\overline{U}_e = \frac{\overline{\sigma}_{12}^2}{H}\left(\frac{H-2h}{2G_B}+\frac{h}{G_I}\right), \tag{22}$$

where $\overline{\sigma}_{12}$ is the remote applied shear stress. The average defect energy then is simply $\overline{U}_p = \overline{U} - \overline{U}_e$, in accord with relation (10).

Fig. 9 shows DD and SGP estimates for the average defect energy normalised by the total work done $\mathscr{W}$, i.e., $\overline{U}_p/\mathscr{W}$, for (a) $H = 0.5$ μm and $E_I/E_B = 1$, 0.1 and (b) $H = 0.5$, 2 μm and $E_I/E_B = 1$ as a function of the applied shear strain Γ for $h = 0.1$ μm in both cases. In both the DD and SGP formulations, the total work done $\mathscr{W}$ amounts to the area under the corresponding stress–strain curves shown in the previous figures. By applying the above definitions in the present study, we observe in Fig. 9 that the SGP and DD results are in good agreement for both the small and large specimens. In particular, we observe that in the smaller specimen ($H = 0.5$ μm) with $E_I/E_B = 1$ the amount of energy stored in the elastic fields of the GNDs (defect energy) can be as much as 30% of the total work done. This portion reduces to the value of 10% as the Young's moduli ratio E_I/E_B decreases (part (a)) or the specimen height increases (part (b)). Note however that the agreement between the SGP and the DD curve for $H = 2$ μm in part (b) is poor, although they both predict a significant drop of the value of the average defect energy as the crystal height increases from $H = 0.5$ μm to $H = 2$ μm. These observations further suggest that the assumption

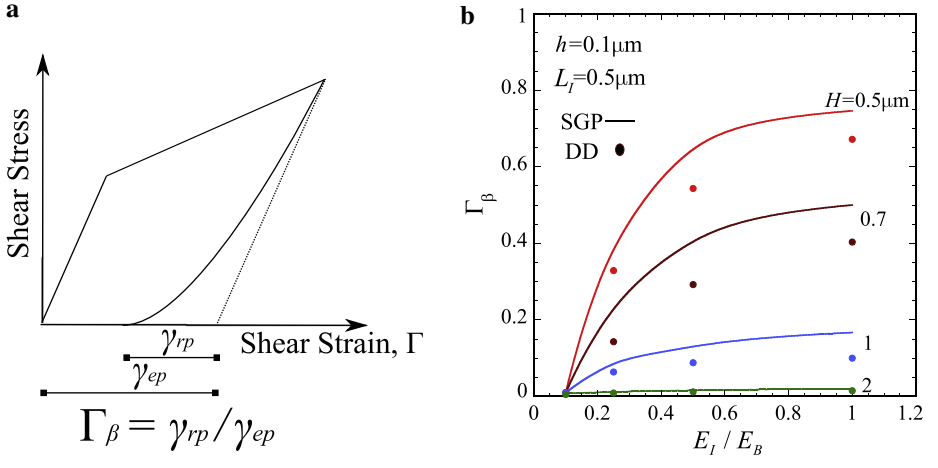

Fig. 8. In part (a), the graphic representation of the normalised reverse shear plastic strain Γ_β is shown. In part (b), collective plots are presented for Γ_β as predicted by the DD (full circles) and the SGP (continuous lines) for $H = 0.5$, 0.7, 1, 2, 4 μm and $h = 0.1$ μm as a function of the Young's moduli ratio E_I/E_B at a total shear strain $\Gamma = 3\%$.

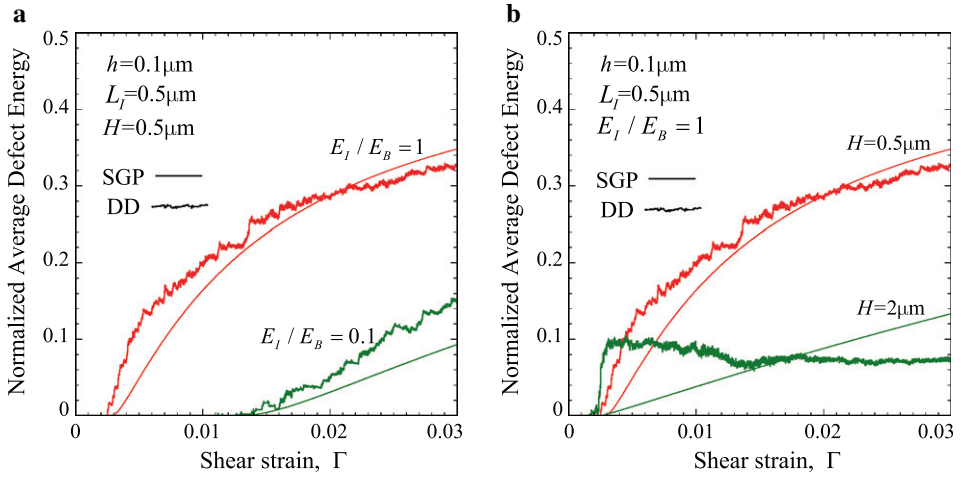

Fig. 9. DD vs. SGP estimates for the average defect energy normalised by the total work done $\overline{U}_p/\mathscr{W}$ for $h = 0.1$ μm and (a) $H = 0.5$ μm and $E_I/E_B = 1$, 0.1 and (b) $H = 0.5$, 2 μm and $E_I/E_B = 1$ as a function of the applied shear strain Γ.

that the local defect energy U_p has a quadratic dependence on the plastic slip $\gamma_{p,i}^{(\alpha)}$ made in the context of the SGP formulation (c.f. (14)) is a fairly good approximation for the sheared single crystal.

3.4. The relative importance of dissipative and energetic terms in the strain gradient formulation

This section presents only SGP results for a sheared single crystal with no interface. The principal aim is to make use of the general constitutive laws of (18) and (19) in order to show the wide range of possible macroscopic constitutive behaviours of the bulk crystal, sandwiched between rigid adherends. The sensitivity of response to particular combinations of energetic and dissipative parts of $q^{(\alpha)}$ and $\tau_i^{(\alpha)}$ is determined. The only relevant length scales are the energetic L/H and the dissipative l/H as introduced in (14) and (16), respectively. Use is made of the material parameters presented in Section 3.2 for the bulk solid and all calculations are presented for an applied loading rate $\dot{\Gamma} = 10^{-3}\ \mathrm{s}^{-1}$. The one difference is that while the definition (13) for $\gamma_e^{(\alpha)}$ is still used with $\rho = 2$, the flag Θ (introduced in (13)) is set equal to either 0 or 1 depending on the case being analysed as specified below.

Table 1 presents all possible combinations of the terms $q^{E(\alpha)}$, $\tau_i^{E(\alpha)}$ and $\tau_i^{D(\alpha)}$. The indicative numbers "1" and "0" serve to denote whether a term is *active* or *inactive*, respectively, in the constitutive description of the material. On the other hand, conventional large-scale plasticity has always a dissipative character, and for this reason the term $q^{D(\alpha)}$ has been set *active* in all cases considered here. In addition, the effect of each term of Table 1 on the macroscopic response of the crystal becomes more clear if no dissipative hardening is assumed; hence, the yield stress σ_y is taken to be independent of plastic strain.

The first two cases in Table 1 correspond to conventional perfectly plastic (von Mises) solids with no kinematic hardening (Case I) and with kinematic hardening (Case II). In Case I, only the term $q^{D(\alpha)}$ is active, while in Case II kinematic hardening is achieved by the addition of the term $q^{E(\alpha)}$ in the constitutive description of the crystal. In the following plots, Cases I and II correspond to $l/H = L/H = 0$ such that no size effects are present.

The Cases A–F describe solids with size effects in yield and/or in hardening, and the corresponding stress–strain curves are presented in Fig. 10. A size effect in yield strength is achieved via the presence of the term $\tau_i^{D(\alpha)}$ whereas a size effect in hardening is due to the term $\tau_i^{E(\alpha)}$. More specifically, the following cases are considered below:

- *Case A:* First, we activate only $\tau_i^{D(\alpha)}$ (i.e., $L/H = 0$ and $\Theta = 0$) which leads to size effects in the yield point, but absent kinematic or gradient hardening.

Table 1
Constitutive description of solids exhibiting size effects.

Cases	$\tau_i^{D(\alpha)}$	$q^{E(\alpha)}$	$\tau_i^{E(\alpha)}$	Size effect on yield	Size effect on hardening
I. Conventional von Mises solid	0	0	0	–	–
II. Conventional kinematic hardening solid	0	1	0	–	–
A. Purely dissipative gradient solid	1	0	0	✓	–
B. Purely gradient hardening solid	0	0	1	–	✓
C. Dissipative gradient solid with conventional kinematic hardening	1	1	0	✓	–
D. Conventional dissipative solid with kinematic and gradient hardening	0	1	1	–	✓
E. Dissipative gradient solid with purely gradient hardening	1	0	1	✓	✓
F. Fully coupled solid	1	1	1	✓	✓

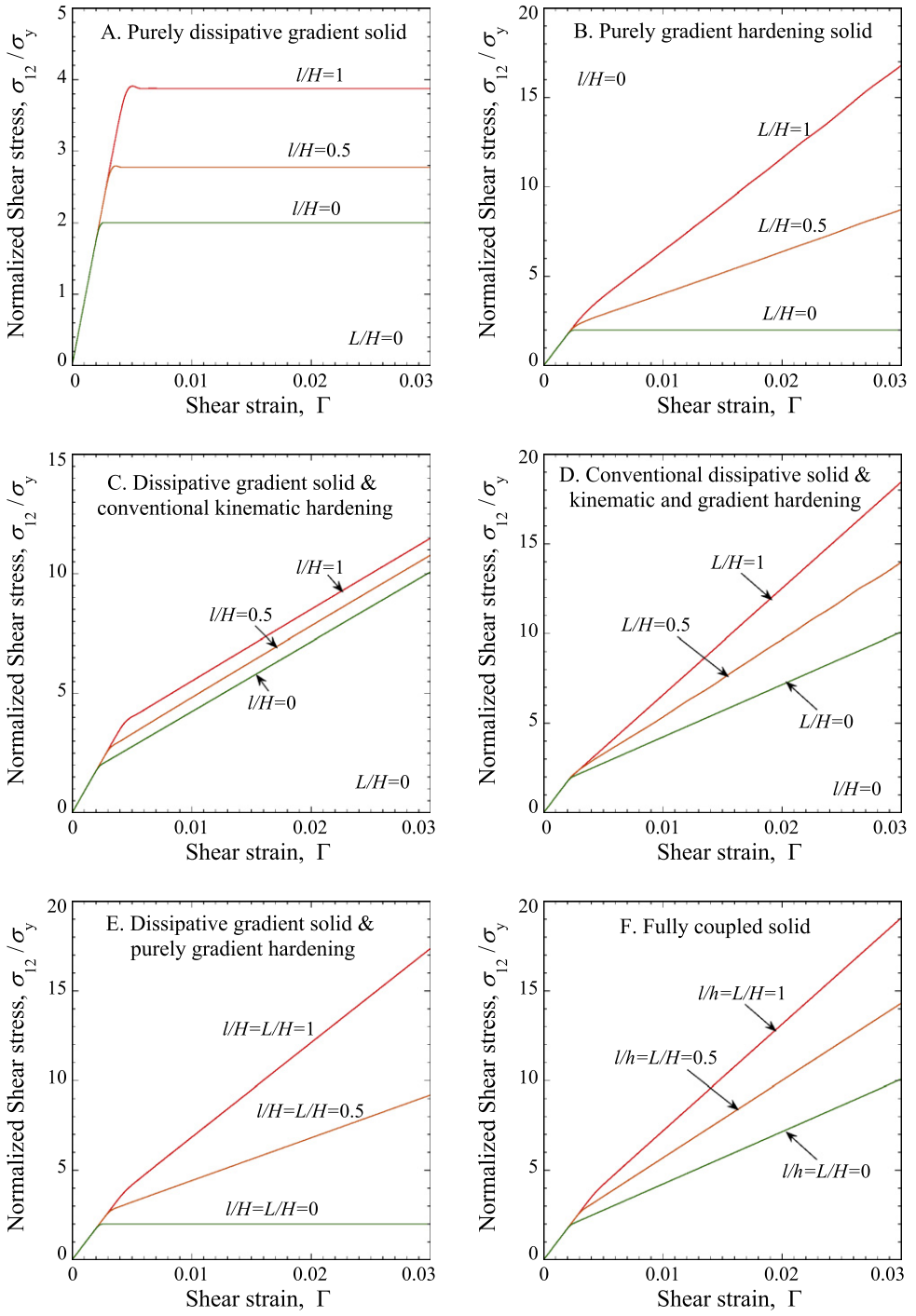

Fig. 10. Normalised SGP shear stress–strain curves for different choices of the constitutive parameters. The labelling of the sub-figures is done according to Table 1.

- *Case B:* By activating only $\tau_i^{E(\alpha)}$ (i.e., $l/H = 0$ and $\Theta = 0$), the solid exhibits only a size effect in hardening (termed gradient hardening). In this case, we note an increase of the macroscopic hardening slope with increasing L/H.
- *Case C:* Here the only inactive term is $\tau_i^{E(\alpha)}$ (i.e., $L/H = 0$ and $\Theta = 1$). The presence of the term $q^{E(\alpha)}$ leads to kinematic hardening, however the slope of hardening remains the same for all l/H since the term $\tau_i^{E(\alpha)}$ is switched off. In addition, a size effect in the yield point is observed.
- *Case D:* Both $q^{E(\alpha)}$ and $\tau_i^{E(\alpha)}$ are active with $\tau_i^{D(\alpha)}$ inactive (i.e., $l/H = 0$ and $\Theta = 1$). Consequently, the crystal exhibits both kinematic and gradient hardening but no size effect in the yield point.

- *Case E:* The presence of $\tau_i^{D(\alpha)}$ and $\tau_i^{E(\alpha)}$ (with $q^{E(\alpha)}$ being inactive; i.e., $\Theta = 0$) gives rise to size effects in yield and hardening with no conventional kinematic hardening. This choice is the most appropriate one for mimicking the DD simulations described in the previous sections.
- *Case F:* All terms are active (i.e., $\Theta = 1$) and consequently the solid is fully coupled, exhibiting size effects in yield as well as kinematic and gradient hardening.

4. Concluding remarks

In this study use has been made of discrete dislocation (DD) and strain-gradient plasticity (SGP) formulations to carry out a plane-strain analysis of a sandwiched sheared single crystal whose upper and lower surfaces are bonded to rigid blocks via interfaces of finite height. The sensitivity of size effects to the interface compliance has been emphasised. The strain-gradient crystal plasticity results were found to be in very good agreement with the discrete dislocation simulations in all cases considered. When the interface is more compliant than the bulk crystal, both the size effect in macroscopic shear strength and the Bauschinger effect are considerably reduced. In addition, a negligible size effect is observed for the initial yield point for all values of interface compliance.

In the case of small crystals with interfaces that have the same Young's modulus as that of the bulk solid, the observed hardening has an energetic character and is attributed to the fact that the fixed upper and lower surfaces (passivated boundary) do not allow the dislocations to exit the crystal thus creating dislocation pile-ups near the boundaries of the specimen. These dislocation pile-ups generate long range elastic back-stresses which impede further dislocation activity and consequently strong plastic strain-gradients develop near the upper and lower boundaries. This in turn increases the internal stored energy in the specimen and leads to strong hardening and significant Bauschinger effects. On the other hand, the presence of an interface with a modulus less than that of the bulk material, results in the relaxation of the elastic back-stresses due to the dislocation pile-ups and consequently in a significant reduction of both the predicted plastic size effect and the Bauschinger effect. Independent experimental measurements of the interface compliances are required in order to check the validity of the hypothesis presented here – this is a topic for future experimental studies.

Finally, the strain-gradient plasticity formulation was used to give a broad range of structural responses for the sandwiched single crystal in shear. A number of these constitutive behaviours cannot at present be modelled in a comprehensive manner by discrete dislocation simulations (such as forest hardening and relaxation of stresses by cross-slip). These complex dislocation phenomena are described in a phenomenological manner by the strain-gradient plasticity theories via the introduction of dissipative and energetic constitutive terms, as described in Section 3.4. Several combinations of the relevant constitutive parameters have been combined in order to obtain a wide range of possible size effects in yield and in hardening. There is a need for experimental studies in order to reveal the most pertinent constitutive law.

Acknowledgement

The authors are grateful to the EPSRC for financial support in the form of Contract No. EP/C52392X/1.

References

Aifantis, K.E., Willis, J.R., 2005. The role of interfaces in enhancing the yield strength of composites and polycrystals. J Mech. Phys. Solids 53, 1047–1070.
Asaro, R.J., 1983. Micromechanics of crystals and polycrystals. Adv. Appl. Mech. 23, 1–115.
Ashby, M.F., 1970. The deformation of plastically non-homogeneous materials. Philos. Mag. 21, 399–424.
Balint, D.S., Deshpande, V.S., Needleman, A., Van der Giessen, E., 2005. A discrete dislocation plasticity analysis of grain-size strengthening. Mater. Sci. Eng. A 400, 186–190.
Benzerga, A.A., Bréchet, Y., Needleman, A., Van der Giessen, E., 2004. Incorporating three-dimensional mechanisms into two-dimensional dislocation dynamics. Modell. Simul. Mater. Sci. Eng. 12, 159.
Borg, U., 2007. Strain gradient crystal plasticity effects on flow localization. Int. J. Plasticity 23 (8), 1400–1416.
Borg, U., Fleck, N.A., 2007. Strain gradient effects in surface roughening. Modell. Simul. Mater. Sci. Eng. 15, S1–S12.
Deshpande, V.S., Needleman, A., Van der Giessen, E., 2002. A discrete dislocation analysis of near-threshold fatigue crack growth. Acta Mater. 49, 3189–3203.
Deshpande, V.S., Needleman, A., Van der Giessen, E., 2002. Discrete dislocation modelling of fatigue crack growth. Acta Mater. 50 (4), 831–846.
Fleck, N.A., Hutchinson, J.W., 2001. A reformulation of strain gradient plasticity. J. Mech. Phys. Solids 49, 2245–2271.
Fleck, N.A., Muller, G.M., Ashby, M.F., Hutchinson, J.W., 1994. Strain gradient plasticity: theory and experiment. Acta Metall. Mater. 42, 475–487.
Fleck, N.A., Willis, J.R., 2009a. A mathematical basis for strain gradient plasticity theory. Part I: scalar plastic multiplier. J. Mech. Phys. Solids 57, 161177.
Fleck, N.A., Willis, J.R., 2009b. A mathematical basis for strain gradient plasticity theory. Part II: tensorial plastic multiplier. J. Mech. Phys. Solids 57, 10451057.
Gurtin, M.E., 2002. A gradient theory of single-crystal viscoplasticity that accounts for geometrically necessary dislocations. J. Mech. Phys. Solids 50, 5–32.
Gurtin, M.E., Needleman, A., 2005. Boundary conditions in small-deformation, single-crystal plasticity that account for the Burgers vector. J. Mech. Phys. Solids 53, 1–31.
Hirth, J.P., Lothe, J., 1968. Theory of Dislocations. McGraw-Hill, New York.
Hussein, M.I., Borg, U., Niordson, C.F., Deshpande, V.S., 2008. Plasticity size effects in voided crystals. J. Mech. Phys. Solids 56, 114–131.
Hutchinson, J.W., 2000. Plasticity at the micron scale. Int. J. Solids Struct. 37, 225–238.
Kubin, L.P., Canova, G., Condat, M., Devincre, B., Pontikis, V., Bréchet, Y., 1992. Dislocation microstructures and plastic flow: a 3D simulation. Solid State Phenom. 2324, 455–472.
Michel, J.C., Moulinec, H., Suquet, P., 1999. Effective properties of composite material with periodic microstructure: a computational approach. Comput. Methods Appl. Mech. Engrg. 172, 109–143.
Nye, J.F., 1957. Physical Properties of Crystals. Oxford University Press Inc., New York.

Rice, J.R., 1987. Tensile crack tip fields in elastic-ideally plastic crystals. Mech. Mat. 6, 317–335.
Shu, J.Y., Fleck, N.A., Van der Giessen, E., Needleman, A., 2001. Boundary layers in constrained plastic flow: comparison of nonlocal and discrete dislocation plasticity J. Mech. Phys. Solids 49, 1361–1395.
Tagarielli, V.L., Fleck, N.A., in preparation.
Van der Giessen, E., Needleman, A., 1995. Discrete dislocation plasticity: a simple planar model. Model. Simul. Mater. Sci. Eng. 3, 689–735.
Xiang, Y., Vlassak, J.J., 2006. Bauschinger and size effects in thin-film plasticity. Acta Mater. 54, 5449–5460.